Implementation of Synthetic Cloud Fields for PV Modeling in Distribution Grid Simulations

Matthew Lave, Matthew J. Reno, Robert J. Broderick
Sandia National Laboratories, Livermore, CA and Albuquerque, NM, 94550 and 87185, USA

***Abstract* — The method for creating synthetic high-frequency solar simulations with unique profiles for each interconnection point on a distribution system feeder using low-frequency input data is presented, including recent improvements which have made it more accurate at matching measured irradiance statistics. These synthetic cloud fields can then be implemented into distribution grid simulations to model irradiance profiles for locations across the feeder. Without unique PV inputs at each interconnection point, the number of voltage regulator tap change operations is significantly overestimated.**

I. Introduction

High-frequency solar variability with unique inputs for different interconnection points on distribution feeders are important inputs to accurate quasi-static time series (QSTS) distribution grid integration studies. Using low-frequency solar variability results in underestimation of the impact of solar photovoltaics (PV) to distribution grid operations, while using a single PV profile for all interconnection points results in an overestimation of the PV impact due to the spatial smoothing provided by distributed PV.

However, measurements of high-frequency solar variability are scarce, and so methods which can synthetically generate high-frequency data from more ubiquitous low-frequency data such as satellite-derived irradiance are desired. In this paper, we demonstrate how synthetic cloud fields which match high-frequency irradiance statistics can be integrated into distribution grid QSTS simulations. These synthetic cloud fields allow for unique PV samples at each interconnection point, samples which accurately represent the high-frequency solar variability statistics while also capturing the spatial decorrelation (i.e., not all PV modules see clouds at the exact same time).

II. Synthetic Cloud Field Method

The basic method to produce synthetic cloud fields was presented previously [1]. The synthetic cloud fields method begins by creating random noise at different spatial scales. Next, each scale of random noise is linearly interpolated to a grid the same size as the finest grid. This results in a smooth field for the larger scales while retaining the more variable field at the smaller scales. These interpolated fields are added together to create a cloud field. Different weights are applied to the different interpolated field. These weights are related to the solar variability at each timescale: longer term variability (e.g., large, slow passing clouds) will lead to higher weighting on the coarsely interpolated scales, while shorter term variability (e.g., small clouds leading to short fluctuations) will mean higher weighting of the fine scales.

However, this initial cloud field does not look like actual sky conditions: values range from fully clear to fully cloudy without distinct cloud shapes, as seen in Figure 1.

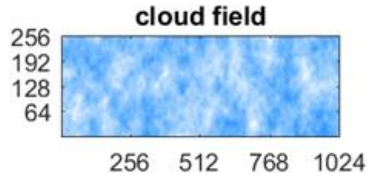

Figure 1: Initial cloud field created by summing all the interpolated fields.

To obtain more distinct clouds, we create a cloud mask, which is based on the expected fraction of the sky covered by clouds, as seen in Figure 2.

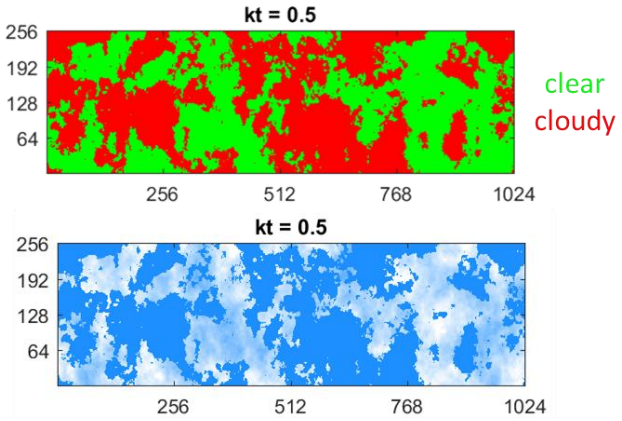

Figure 2: [Top] Cloud mask. [Bottom] Resulting cloud field after mask is applied.

Cloud field values range from 0 to 1 and are analogous to clear-sky index samples. They can be converted to GHI by multiplying by a clear-sky index (e.g., [2]).

In summary, these are the main factors which affect cloud field creation:

A) The weighting of fine versus coarse scales – this impacts the variability of the cloud field.
B) The percentage of the area covered by clouds – this determines how many areas are clear blue sky.
C) The average intensity of clouds – clouds may tend to be opaque or more translucent.

In this work, we will discuss how these factors can be derived from a single high-frequency irradiance sample or approximated from a coarse sample such as an hourly satellite-derived irradiance measurement.

III. Cloud Field Methodology Improvements

The main factors listed in section II. are best derived from a single high-frequency irradiance sample. In this way, the single measurement is extended through the cloud field to create unique PV samples at each point over an area, such as the area of a distribution feeder. In this section, we discuss the previous implementation (described in [1]) which can be applied to low-frequency (e.g., hourly) irradiance inputs, and recent improvements made to the implementation to incorporate high-frequency (e.g., 1-second) irradiance inputs which result in more accurate irradiance statistics across the synthetic cloud fields.

A. Scale Weighting

Under the previous implementation, the weighting of fine versus coarse cloud field scales (factor A) was a monotonic function of the variability score. Scaling weights increased significantly at higher order (coarser) timescales, and thus often resulted in large cloud features dominating leading to sharp edges and higher than expected solar variability. Additionally, under the previous implementation only 8 (coarse to smooth) cloud field scales were considered. Recent improvements implemented spatial scale weighting based on a wavelet transform of the measurements from a point irradiance sensor and increased the cloud field scales to 12 to be consistent with the temporal scales computed based on a wavelet transform [3] of the input high-frequency irradiance.. This results in cloud field scale weighting that is not necessarily monotonically increasing and can better capture variation among the timescales, as seen in Figure 3.

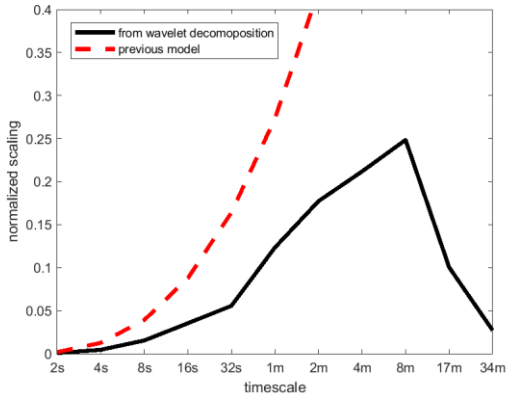

Figure 3: Normalized scaling of cloud fields using a wavelet decomposition (black line), showing the enhanced detail versus the previous simple model (red dashed line).

B. Clear-Sky Fraction

The fraction of clear-sky areas (factor B) was previously computed from the average clear-sky index of the irradiance sample. This often resulted in an over-prediction of the areas of clear-sky. For example, a fully cloudy period of varying cloud opacities (say from 0.3 to 0.7) may result in an average clear-sky index of 0.5. Although this period was fully cloudy, the previous method assumed that 50% of the area was clear-sky. Improvements were implemented to instead account for clear periods based on the percentage of values in the measured timeseries which had a clear-sky index greater than 0.9. In this way, the percentage of clear-sky pixels is decoupled from the average clear-sky index.

C. Cloud Opacity

Two additional enhancements were made to cloud intensities. First, the new implementation now allows for cloud enhancement – values greater than 1. Cloud enhancement is programmed to only occur at cloud edges – the interface between cloudy areas and clear areas (edges of the cloud mask). Second, the intensity of clouds is scaled to match the average clear-sky index.

Figure 4 compares the ramp rates of the clear-sky index for the improved ("new") and previous ("old") methods to the measured clear-sky index from a high-frequency irradiance sensor in Oahu, Hawaii. This also shows that the new method outperforms the old method, especially during periods of large clouds such as hours 10 and 12. Not shown in Figure 4 is that the improved method also accurately matches ramp rate distributions during very (but not fully) clear conditions during hours 16 and 17 (see Figure 5), while the old method had assumed fully clear conditions and hence that all ramps had zero magnitude.

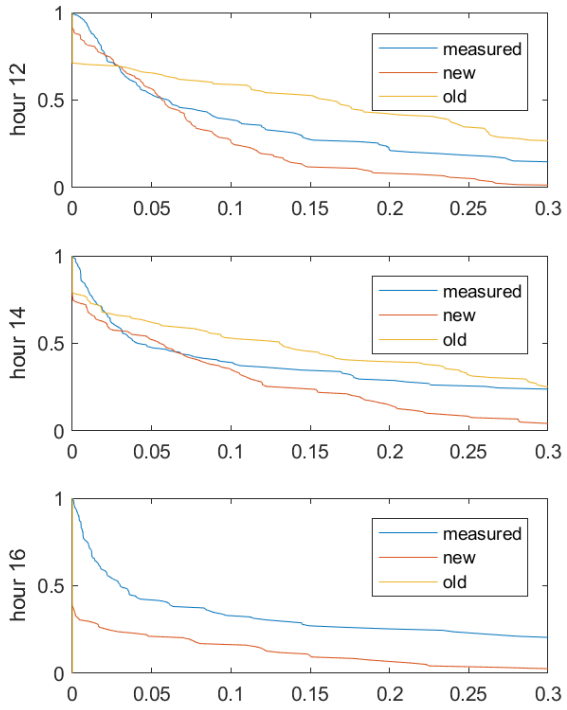

Figure 4: Ramp rate statistics for the measured clear-sky index, and for the method with improvements ("new") and the previous method ("old").

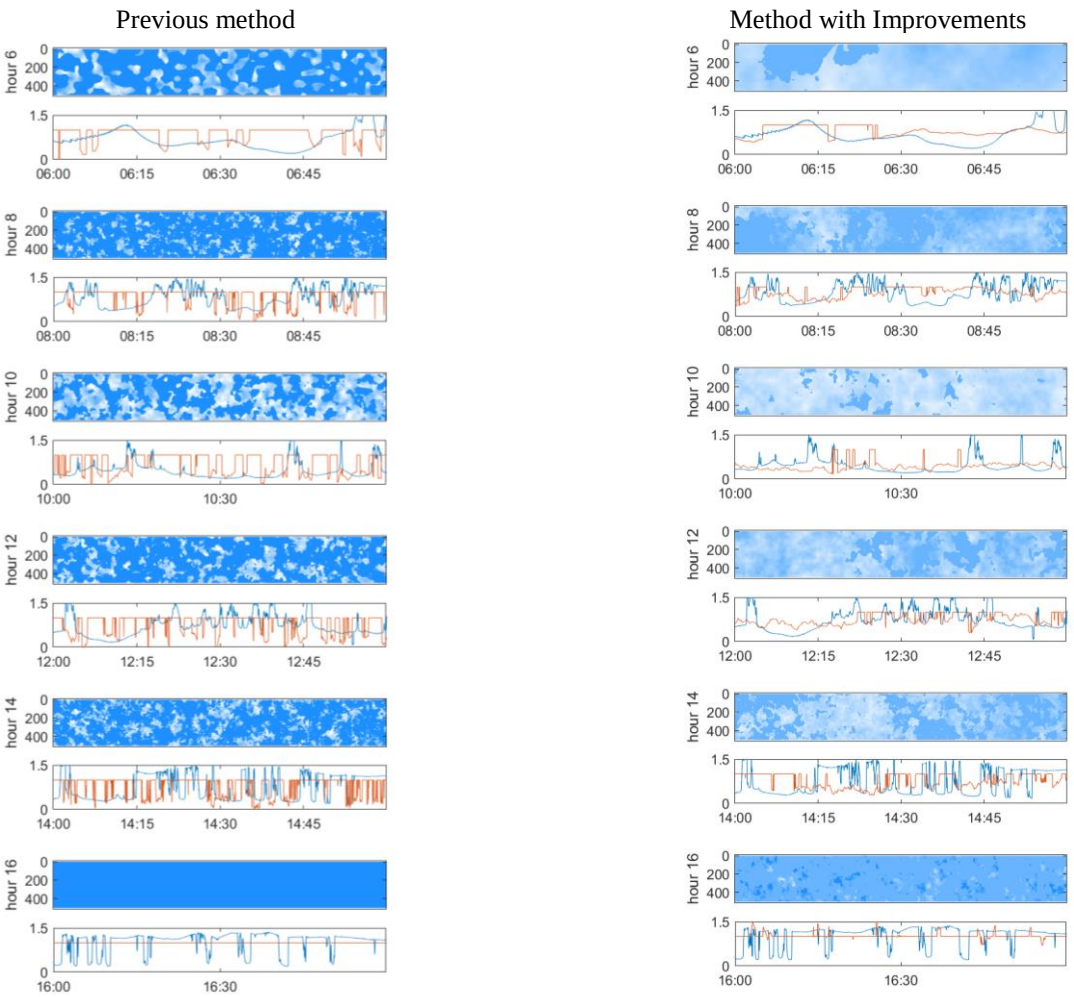

Figure 5: Comparison of cloud fields and clear-sky index samples for the old method to the new method. The blue line is the measured clear-sky index and the red line is the modeled clear-sky index.

Figure 5 shows the cloud fields created with the previous method versus the method with the described improvements. Also included are clear-sky indices derived from the cloud fields compared to the measured clear-sky index. The new method better matches the clear-sky index trends of the measured data. The improved method is much better at capturing the long, continuous cloud features such as those present at hour 6 and hour 10.

IV. Implementation of Cloud Fields into Distribution Grid Studies

Cloud fields were applied to produce unique PV power output profiles for use in quasi-static timeseries (QSTS) distribution grid impact studies, as outlined in the flow chart in Figure 6. First, the PV locations on the feeder to be simulated are mapped to the cloud field. Next, the cloud field is advected through time based on the cloud speed – a constant cloud speed is assumed for the entire cloud field, and for simplicity clouds shapes are static (i.e., the is no deformation or creation of clouds). For each PV location, the passing clear-sky index values are recorded as a timeseries. These clear-sky index timeseries are then translated to create a simulated irradiance timeseries by multiplying by a clear-sky irradiance model. Finally, the simulated irradiance timeseries are passed through DC (i.e., PV module characteristics) and AC (i.e., inverter characteristics) power models to create simulated AC power output at each PV interconnection location.

These unique PV power output profiles were applied to distribution grid simulations using the modeling software OpenDSS. We chose an agricultural distribution feeder with 265 different transformers with PV interconnections as our test feeder, as shown in Figure 7. As seen in Figure 7, the feeder has a voltage regulator tap changer roughly halfway down its main line, allowing for direct quantification of the impact of various PV power profiles to voltage fluctuations. So that the voltage regulator is a better indicator of the PV impact, all PV was located downstream of the voltage regulator.

A total of 2.8MW of PV was connected over the 265 different transformers, corresponding to roughly two 5kW PV systems installed per transformer. Without PV, the maximum load through the voltage regulator was 3.6MW. Load from the peak load week was used for all simulations.

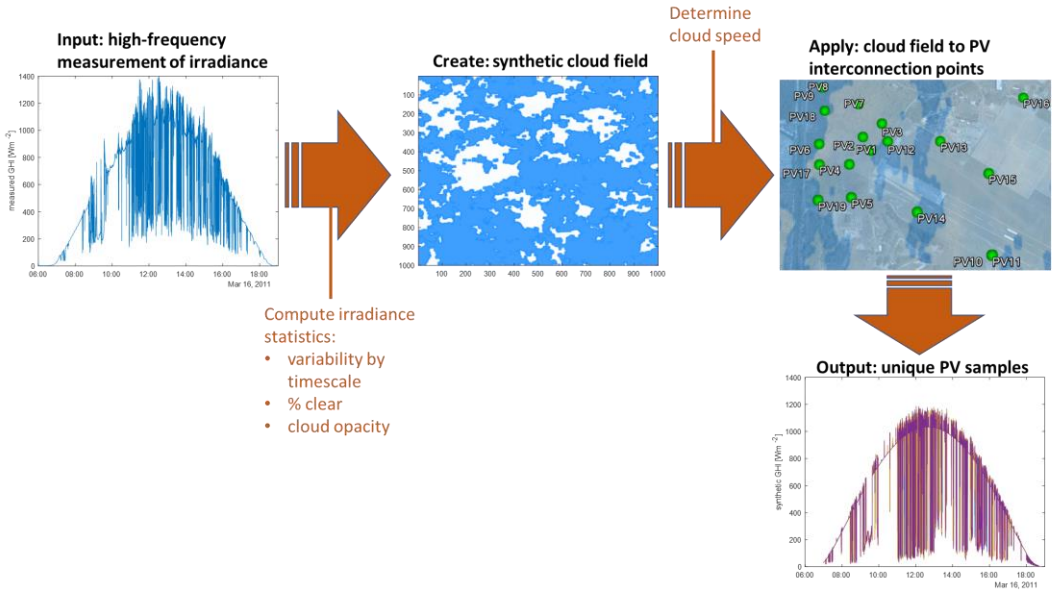

Figure 6: Flow chart showing process to use cloud fields to make unique PV samples across a distribution feeder.

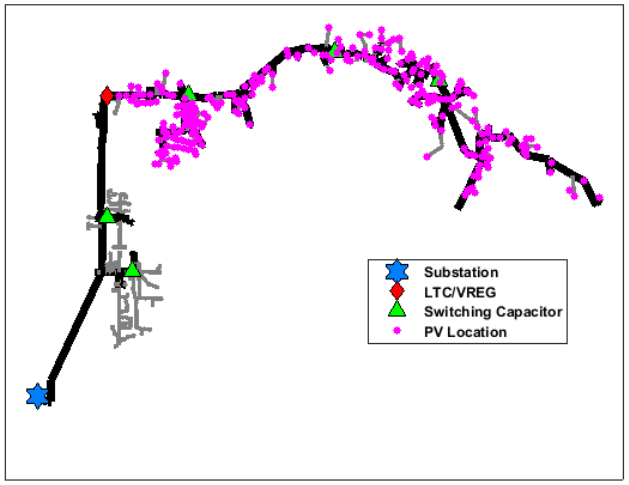

Figure 7: Test feeder layout showing substation (blue star), voltage regulator (red diamond), and the 265 PV interconnection locations (magenta dots).

Two test cases were considered: (a) a comparison of simulations with cloud fields to simulations using a network of irradiance measurements, and (b) a comparison of cloud field simulations to simulations based on only a single irradiance measurement.

A. Cloud Fields vs. Irradiance Measurement Network

To compare the results of the cloud fields to actual measured irradiance, the measurements from the irradiance network in Oahu, HI were used [4]. There are 19 irradiance sensors in the Oahu network, however 2 of the sensors were found to often have bad data and so were eliminated from the analysis. The remaining 17 sensors were used and assigned to one of the PV interconnection points on the feeder. This resulted in many duplicate PV profiles – as there were only 17 unique profiles but 265 interconnection points – but is the best approximation that can be done with only 17 sensors. To mimic this setup, only 17 synthetic irradiance samples derived from cloud fields were used.

Results of this simulation for one week are shown in Figure 8. The synthetic irradiance simulation does a good job of capturing the actual variability of the measured irradiance. The total number of tap change operations over the week is consistent to within 10% between the measured and the synthetic irradiance samples, showing good agreement.

B. Cloud Fields vs. Single Sensor

Cloud fields are created on the presumption that a single irradiance sensor, even at high temporal frequency, does not capture the spatial diversity across a distribution feeder. In other words, a single irradiance sensor applied as the irradiance profile at all transformer will overestimate the variability on the feeder. The realization of this assumption is shown in Figure 9, where one irradiance measurement applied to all transformers is compared to synthetic profiles which are unique at each transformer.

The difference between the single sensor and the 265 unique profile is clear: the single sensor applied to all transformers results in nearly double the number of tap change operations as the 265 unique profiles. The 265 unique profiles, although synthetic, are a more realistic representation of the actual PV impact since they account for the spatial smoothing.

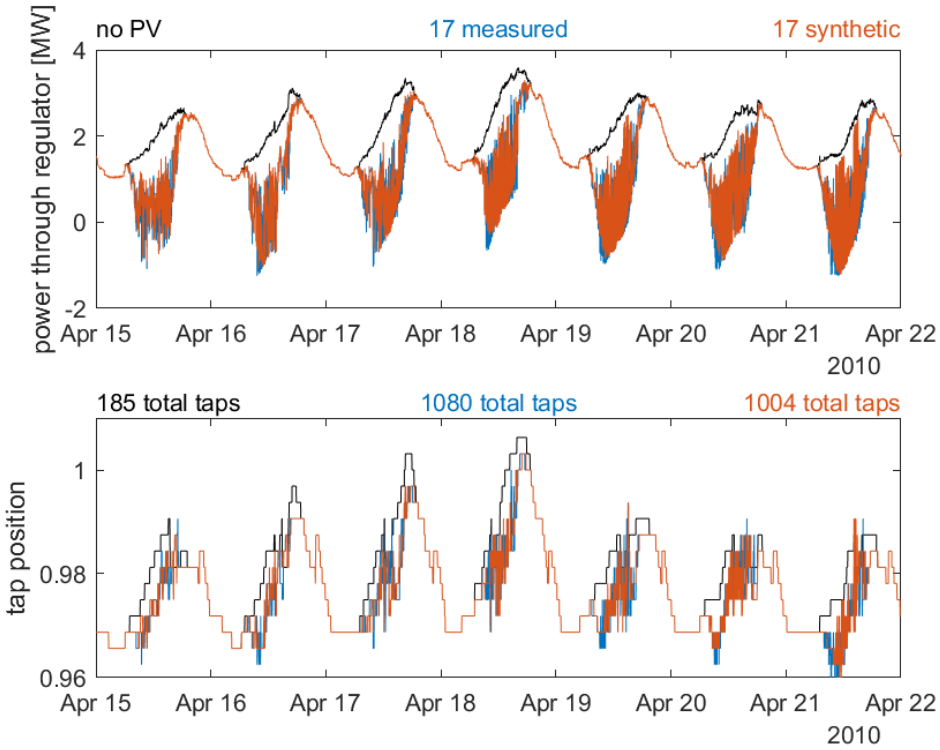

Figure 8: Simulation results when using 17 measured (blue) and 17 synthetic (red) PV inputs. Also included for reference is the no PV case (black).

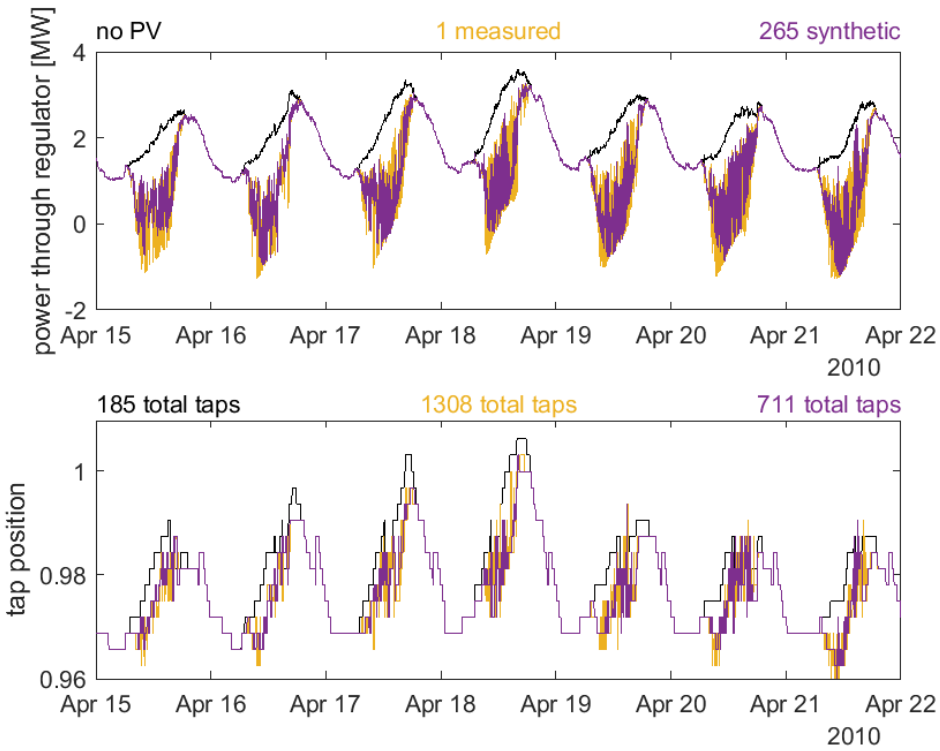

Figure 9: Simulation results when using 1 measured (yellow) and 265 synthetic (magenta) PV inputs. Also included for reference is the no PV case (black).

It is also notable how many fewer tap change operations resulted in the 265 unique profile case (Figure 9) compared to the 17 unique profile case (Figure 8). Although there was smoothing (compared to the single sensor) for the 17 profile case, there was significant additional smoothing for the 265 profiles. This emphasizes how important it is to accurately model the number of unique PV locations – even a relatively dense sensor network (as in the 17 sensor Oahu network) can still significantly underestimate the spatial smoothing.

V. Conclusions

Even at the short distances on a distribution feeder, there can be a significant amount of geographic smoothing between different PV systems, therefore a single irradiance profile cannot be used to model all distributed PV systems on a feeder. The paper demonstrates a more accurate method for modelling the impacts of PV interconnections by using synthetic cloud fields to provide unique irradiance profile for distributed PV with the appropriate levels of correlations between systems based on their distance separation.

In this paper, improvements over the previous method were presented which increase the accuracy of the synthetic cloud fields. Improvements included more accurate, wavelet-based variability scaling, allowance for cloud enhancement, and adjustments to cloud opacity to better match input statistics. The cloud fields were then used to produce PV inputs for distribution grid studies.

The results of these distribution grid studies first compared the results of the synthetic cloud fields to a network of 17 irradiance sensors, as a form of validation. Synthetic results compared well to the actual sensors, which tap change operations within 10%. Next, the synthetic cloud fields were used to create PV profiles at the 265 different transformers with PV on the feeder. Results of this distribution grid simulation were compared to results using only a single measured sensor as input, showing the significant overestimation of PV variability that can occur when using a single measurement (due to not accounting for spatial diversity), thus motivating the need for the synthetic cloud fields presented in this paper.

Acknowledgment

Sandia National Laboratories is a multimission laboratory managed and operated by National Technology and Engineering Solutions of Sandia, LLC, a wholly owned subsidiary of Honeywell International, Inc., for the U.S. Department of Energy's National Nuclear Security Administration under contract DE-NA0003525. Report number SAND2018-6325 C.

References

[1] M. Lave, M. J. Reno, and R. J. Broderick, "Creation and Value of Synthetic High-Frequency Solar Inputs for Distribution System QSTS Simulations," presented at the IEEE PVSC 44, Washington, D.C., 2017.

[2] P. Ineichen and R. Perez, "A new airmass independent formulation for the Linke turbidity coefficient," (in English), *Solar Energy,* vol. 73, no. 3, pp. 151-157, 2002.

[3] M. Lave, J. Kleissl, and E. Arias-Castro, "High-frequency irradiance fluctuations and geographic smoothing," *Solar Energy,* vol. 86, no. 8, pp. 2190-2199, 8// 20

[4] Sengupta, M.; Andreas, A. (2010). Oahu Solar Measurement Grid (1-Year Archive): 1-Second Solar Irradiance; Oahu, Hawaii (Data); NREL Report No. DA-5500-56506. http://dx.doi.org/10.5439/1052451